

# Signatures of fractionalization in the field orientation dependent spin dynamics of the Kitaev honeycomb model

David C. Ronquillo and Nandini Trivedi

*Department of Physics, The Ohio State University, Columbus Ohio 43210, USA*

(Dated: June 22, 2022)

The main question we address is how to probe the fractionalized excitations of a quantum spin liquid, for example, in the Kitaev honeycomb model. We propose distinct signatures in the dynamical response of the spin-spin correlation function and its dependence on the magnitude and direction of a magnetic field in order to distinguish different phases. For antiferromagnetic (AF) Kitaev exchange couplings, the observed level crossing develops a gap as the field is rotated from the [111] to the [001] direction. Also, the large number of modes in the dynamical response are greatly reduced as the field is rotated toward [001] resulting in a clearly discernible beating pattern in the time-dependent spin-spin correlation function, possibly observable in pump-probe experiments. We further observe a change in the nature of the lowest lying excitations from single spin-flips for fields along [111], to double spin-flips for fields along [001]. Finally, via an analysis of the plaquette flux operator, we determine the field strength and orientation dependence of the non-Abelian Kitaev quantum spin-liquid phase, the enigmatic intermediate phase (for AF couplings only), and the partially polarized phase. Our results are obtained using exact diagonalization on finite clusters with periodic boundary conditions.

PACS numbers:

## I. INTRODUCTION

Signatures of the exotic fractionalized excitations of the two-dimensional Kitaev model on a honeycomb lattice have recently been of interest given their experimental accessibility within candidate Kitaev-like materials [1–3]. The exactly solvable Kitaev model consists of  $S = 1/2$  degrees of freedom that are frustrated by anisotropic bond-dependent, nearest-neighbor, interactions

$$H_K = \sum_{\alpha} \sum_{\langle j,k \rangle_{\alpha}} J_{\alpha} \sigma_j^{\alpha} \sigma_k^{\alpha}, \quad (1)$$

where  $J_{\alpha}$  is the Kitaev exchange constant,  $\alpha \in \{x, y, z\}$ ,  $j$  and  $k$  are nearest-neighbor sites lying along the bond  $\alpha$ , and  $\sigma_j^{\alpha}$ ,  $\sigma_k^{\alpha}$  are corresponding Pauli matrices [4].

Recent theoretical advances suggest inelastic neutron scattering as revealing identifying characteristics of fractionalized excitations in the dynamical structure factor of candidate Kitaev materials [5, 6], while measuring the heat capacity of these materials may show characteristic features of fractionalization via an analysis of a system's entropy release [7]. These advances reflect an attempt to shed light on the nature of the Kitaev quantum spin-liquid (QSL) ground state, whose fractionalized excitations within the gap induced non-Abelian phase may find application in possible quantum computing devices [8].

Originally conceived as a toy model, researchers have gone on to consider the microscopic mechanisms necessary for realizing Kitaev physics in real materials. This has led to proposals of extended Kitaev-Heisenberg Hamiltonians [9–11], as well as Hamiltonians having additional symmetric off-diagonal interactions [12, 13]. The

original theoretical predictions concerning the dynamical response and temperature dependence of thermodynamic quantities of the pure Kitaev model were experimentally investigated on the candidate compounds  $\alpha$ -RuCl<sub>3</sub> [14, 15], and A<sub>2</sub>IrO<sub>3</sub> (A = Na, Li) [16], respectively. The salient features that appear in the data are attributed to the residual fractional excitations of the pure Kitaev phase proximate to these materials' zig-zag ordered ground state. Recently, experimental measurements of the thermal Hall conductivity,  $\kappa_{xy}$ , of  $\alpha$ -RuCl<sub>3</sub> have even revealed signatures of itinerant Majorana excitations in the sign, magnitude, and temperature (T) dependence of  $\kappa_{xy}/T$  for temperatures within the range  $T_N = 7 \text{ K} < T < 80 \text{ K} \sim J_{\alpha}/k_b$ , where  $T_N$  is the temperature at which the zig-zag order onsets [17].

The strong isotropy of the Kitaev interactions in  $\alpha$ -RuCl<sub>3</sub> inevitably led experimental researchers to investigate the physical properties of this material under an externally applied magnetic field, with the aim of observing signatures of the Kitaev model's celebrated gapped non-Abelian fractionalized excitations [18–25]. Recently, much of the theoretical interest has been to perform numerical simulations on extended Kitaev models with an externally applied field, and to try to fit the results of these numerics to the experimental data [26–28].

In this work, we use exact diagonalization on a finite sized cluster to offer an unambiguous signature of fractionalization of spin-flip quanta in the dynamical local spin-spin correlations of the pure Kitaev model as a function of an externally applied magnetic field. Whereas recent attention has been focused on observing a broad continuum in the dynamical structure factor as indicative of the fractional excitations of a non-ordered ground state [5, 6], we propose investigating real time dynamics

of the spin-spin correlations where we expect the signatures of fractionalization to be sharp and distinct. We demonstrate this to be the case here for certain orientations of the externally applied magnetic field coupled to Eq. 2. We also demonstrate clear signatures of fractionalization in the field evolution of the intensity of dominant frequency modes as a function of the Zeeman field's orientation relative to the plain of the honeycomb lattice. We consider both the ferromagnetic (FM) ( $J_\alpha < 0$ ) and antiferromagnetic (AF) ( $J_\alpha > 0$ ) cases of the Kitaev coupling term and demonstrate the consistency of our results with recent claims of an enigmatic intermediate phase for AF interactions [29, 30].

Our main results are the following: (i) We find a level crossing in the energy spectrum of the AF Kitaev honeycomb model under an applied magnetic field pointing along the [111] direction, indicative of a phase transition between an enigmatic intermediate phase and a high field partially polarized phase, detectable in the on-site dynamical response. (ii) We find the opening of a gap at the level crossing point in both the spectrum, and the local dynamical response, by varying the orientation of the applied field away from the [111] direction, and towards the [001] direction. (iii) The dynamical response along [111] is characterized by a plethora of frequency modes across all energies and field strengths. For both AF and FM Kitaev exchange interactions, upon varying the orientation of the applied field from the [111] to the [001] direction, the number of modes is considerably reduced resulting in a clearly discernible beating pattern in the local dynamical correlations between a few modes of comparable strength and energy. (iv) We find that the behavior of the average of plaquette operators,  $\langle W_p \rangle$ , and its dependence on the field strength and orientation provides a useful diagnostic of the non-Abelian Kitaev spin-liquid, intermediate, and polarized phases, and reveals differences between the FM and AF cases.

## II. MODEL AND NUMERICAL APPROACH

We use exact diagonalization on eight to sixteen site clusters with periodic boundary conditions; the eight site cluster consisting of four honeycomb plaquettes, used for most of the work presented here is shown in Fig. 1. In looking to isolate signatures of fractionalization we work with

$$H = \sum_{\alpha} \sum_{\langle j,k \rangle_{\alpha}} J_{\alpha} \sigma_j^{\alpha} \sigma_k^{\alpha} - \vec{h} \cdot \sum_j \vec{\sigma}_j, \quad (2)$$

and resort to the following parametrization

$$J_x = J_y = J_z = J = \pm \cos \theta, \quad (3)$$

$$\vec{h} = \pm(\lambda, \lambda, 1) \sin \theta, \quad (4)$$

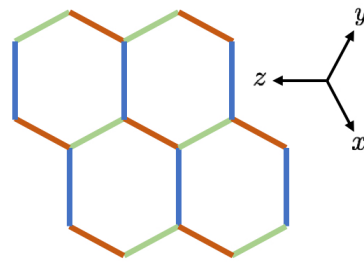


FIG. 1: Eight site cluster consisting of four honeycomb plaquettes having periodic boundary conditions used in our exact diagonalization simulations. Blue bonds correspond to  $z$ -bonds, green bonds correspond to  $x$ -bonds, and red bonds correspond to  $y$ -bonds.

with  $\theta = \tan^{-1}(h_z/J)$ ,  $0 \leq \theta \leq \pi/2$ ,  $0 \leq \lambda \leq 1$ , and the positive (negative) case corresponding to AF (FM) interactions between neighboring spins along respective bonds  $\alpha \in \{x, y, z\}$ . We are thus only considering the physics at the isotropic point of this model's parameter space for fields of varying strength  $\theta$ , and along varying orientations ranging from [111] for  $\lambda = 1$  to [001] for  $\lambda = 0$ .

We are mainly interested in calculating

$$S_{jk}^{\alpha\alpha}(t, h_z, \lambda) = \langle 0_{h_z, \lambda} | \sigma_j^{\alpha}(t) \sigma_k^{\alpha}(0) | 0_{h_z, \lambda} \rangle, \quad (5)$$

where  $|0_{h_z, \lambda}\rangle$  is the field strength and field orientation dependent ground state of Eq. 2, and  $\sigma_j^{\alpha}(t) = e^{iHt} \sigma_j^{\alpha}(0) e^{-iHt}$ . Below, we restrict our calculations to the case of  $j = k$ , and  $\alpha = z$ .

We also calculate the field-dependent on-site time Fourier transform of Eq. 5,

$$\begin{aligned} S_{jk}^{zz}(\omega, h_z, \lambda) &= \int_{-\infty}^{\infty} S_{jk}^{zz}(t, h_z, \lambda) e^{i\omega t} dt \\ &= \sum_n \langle 0_{h_z, \lambda} | \sigma_j^z(0) | n \rangle \langle n | \sigma_k^z(0) | 0_{h_z, \lambda} \rangle \times \\ &\quad \delta(\omega + E_0 - E_n), \end{aligned} \quad (6)$$

where  $n$  is the energy quantum number indexing the various eigenenergies and eigenstates of  $H$ .

Finally, we calculate the average of the expectation values of the four plaquette operators,  $\langle W_p \rangle = \sum_{i=1}^4 W_{p_i} = \sum_{i=1}^4 \prod_{j \in p_i} \sigma_j^{\alpha(j)}$ , with respect to the ground state, for plaquettes  $p_i$  with  $i \in \{1, 2, 3, 4\}$ , and bonds  $\alpha(j)$  emanating from site  $j$  away from the interior of the plaquette. The eigenvalues of  $W_{p_i}$  are  $\pm 1$ , and  $[W_{p_i}, H] = 0$  when  $h_z = 0$ . In this limit, the ground state is known to lie within the  $W_{p_i} = 1$  block for all  $p_i$  [31], and an excitation corresponding to  $W_{p_i} = -1$  for any of the  $p_i$ 's indicates the presence of a flux. The behavior of the plaquette operator indicates the robustness of the Kitaev spin-liquid ground state as a function of the field strength,  $\theta$ , and

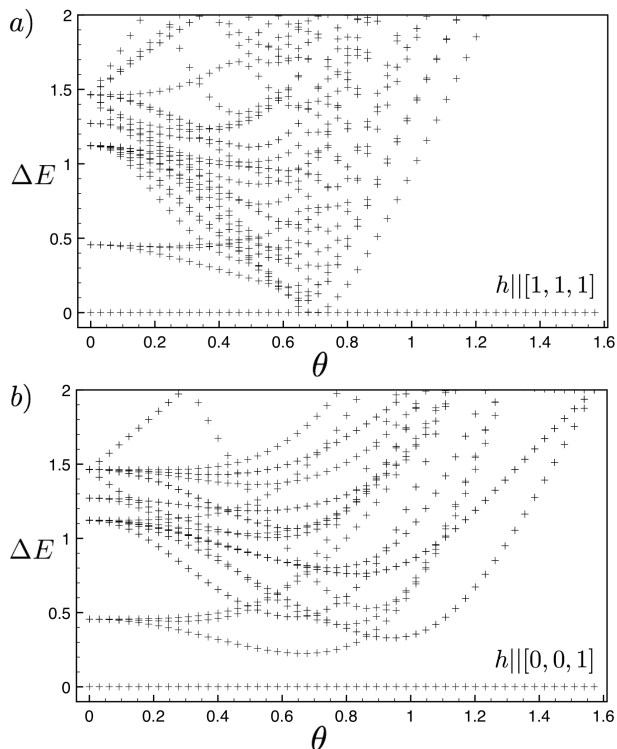


FIG. 2: Energies of the lowest lying excitations of the AF case of Eq. 2 relative to the energy of the ground state as a function of the field strength parameter  $\theta$  for a field pointing along the (a) [111] direction, and, (b) [001] direction. In case (a), the gap between the ground state and the first excited state closes near  $\theta^* \equiv \theta \approx 0.71$ . By changing the orientation of the field away from [111] to [001] in (b), a gap is induced at the formerly gapless point, near  $\theta^*$ , which reaches its maximum value for field along [001].

orientation parameter,  $\lambda$ .

### III. TIME-DEPENDENT SPIN-SPIN CORRELATION FUNCTIONS

#### A. Dynamical Response for Antiferromagnetic ( $J > 0$ ) Couplings

Field along [111]: For the AF case, Fig. 2 shows the energies of the lowest lying excitations relative to the energy of the ground state as a function of the field strength parameter,  $\theta$ . For the field pointing along [111], there is a clear level crossing near  $\theta^* \approx 0.71$ . As the field is rotated by changing  $\lambda$  away from unity, a gap is induced in the spectrum at  $\theta^*$  that reaches its maximum value at  $\lambda = 0$ .

The presence of a gap is reflected in the on-site, time Fourier transform, Eq. 6, displayed in Fig. 3. We notice the onset of two main modes at  $\theta = 0$  for energy gap values  $\Delta E \approx 1.46$  and  $\Delta E \approx 5.46$ . Upon increasing

$\theta$  these modes split into various smaller modes having their own independent trajectories.

While the ground state, as expected, has no flux with  $\langle W_p \rangle = 1$ , the excited states  $\Delta E$  have  $\langle W_p \rangle = 0$ , implying that for our 4 plaquette cluster, two of the plaquettes in each of these states have  $\langle W_{p_i} \rangle = 1$  while the other two have  $\langle W_{p_i} \rangle = -1$ . This is in agreement with our expectation that the lowest flux excitation for this model detectable via the action of a spin operator (such as those composing the spin correlation function, Eq. 5) should involve a state having a pair of fluxes.

The level crossing observed in the spectrum in Fig. 2a, near  $\theta^* \approx 0.71$  in the  $\lambda = 1$  limit, also leaves an imprint in the dynamical response shown in Fig. 3a. At  $\theta = \theta^*$  the trajectories of various modes below  $\theta^*$  switch from moving toward lower frequency with increasing  $\theta$  to increasing in frequency with increasing  $\theta$ . Importantly, both the level crossing and the behavior of the modes above and below the critical  $\theta$  value suggest, and are consistent with recent claims of, a phase transition between the higher field partially polarized phase and an intermediate phase which is also contiguous to the non-Abelian Kitaev quantum spin-liquid phase at lower  $\theta$ . The transition between the latter two phases at lower  $\theta$  is less discernible given the lack of a level crossing in both the spectrum and the frequency response.

For fields approaching  $\theta = \pi/2$ , the plethora of modes tend toward higher  $\omega$  and finally converge into multiple, well separated, modes. The nature of the excitation corresponding to the lowest of these modes (located near  $\omega/J \approx 3.46$  at  $\theta = \pi/2$ , see Fig. 3a) consists of a single spin flip about the completely polarized state along  $\hat{z}$ .

Dependence on field orientation: Rotating the field from [111] toward [001] has the effect of coupling the field preferentially to bonds perpendicular to the  $\hat{z}$  direction. This opens up a gap in both the spectrum and the on-site time Fourier transform where the level crossing once resided. Also, the plethora of modes that exists for values of  $\lambda$  closer to unity is greatly reduced for lower  $\lambda$  (compare Fig. 3a and b) until at  $\lambda = 0$  we are left with a signal that is much less dense in the number of frequency modes. Although there is now a gap in both the spectrum and the frequency response, we still observe a redirection of a considerable number of the remaining modes. Their frequencies become lower with increasing  $\theta$  below  $\theta \approx 0.71$ , but increase in frequency with increasing  $\theta$  above this value. We also notice that the zero mode along  $\omega/J = 0$  becomes the dominant (i.e. more heavily weighted) mode as we adjust  $\lambda$  from unity to zero. Unlike the  $\lambda = 1$  case, here only a single mode survives up to  $\theta = \pi/2$ , above  $\omega/J = 0$ , after constituent modes converge somewhere above  $\theta \approx 1.2$ . Interestingly, while this latter mode is located near  $\omega/J \approx 3.46$  at  $\theta = \pi/2$  (Fig. 3c), the nature of the excitation here consists of a pair of spin flips in the direction opposite to that of a completely polarized

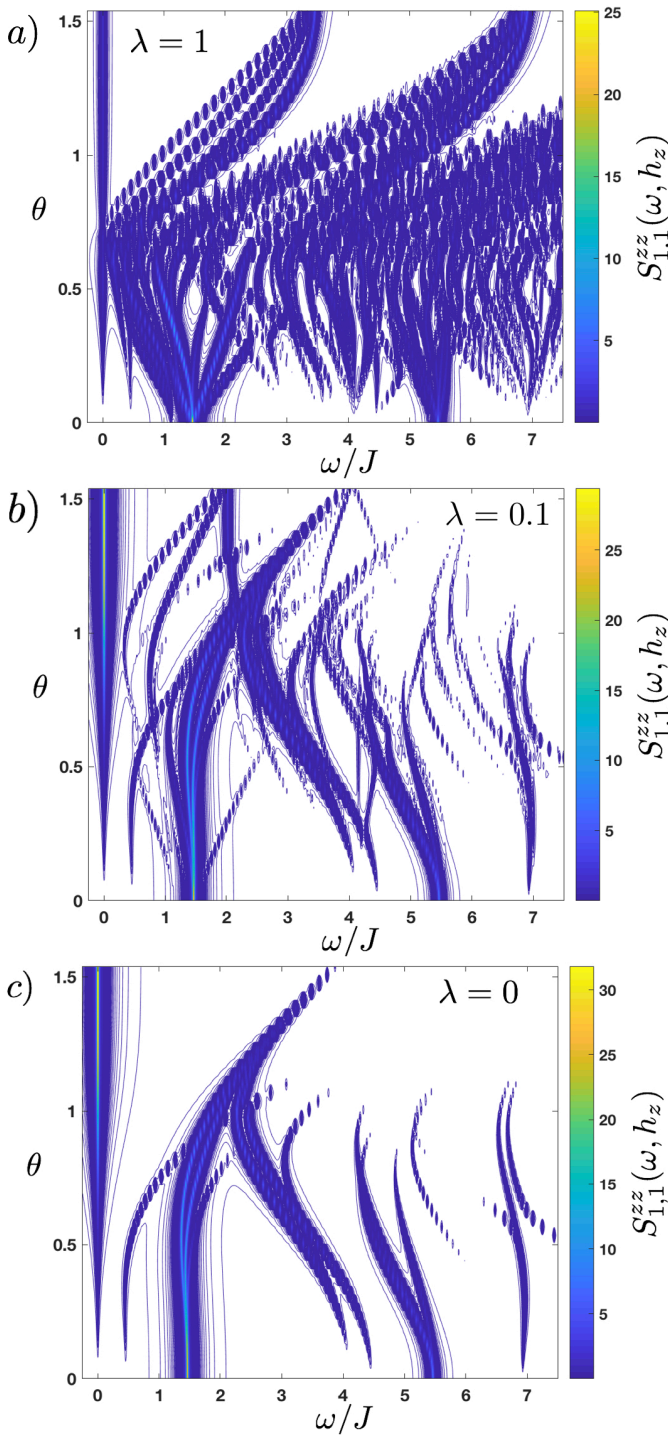


FIG. 3: The on-site dynamical response for the AF case of Eq. 2, calculated using Eq. 6, for values of the field orientation parameter a)  $\lambda = 1$ , b)  $\lambda = 0.1$ , and c)  $\lambda = 0$ . a) For  $\theta < \theta^* \approx 0.71$ , the point at which a level crossing occurs in Fig. 2a, various frequency modes have divergent trajectories across  $\omega$  as a function of  $\theta$ . Above  $\theta^*$ , all trajectories become streamlined and increase with  $\omega$  with increasing  $\theta$ . b) Adjusting the field orientation parameter to  $\lambda = 0.1$  shifts the redirection field  $\theta$  closer to one. c) In the  $\lambda = 0$  limit only a few modes remain visible in the response.

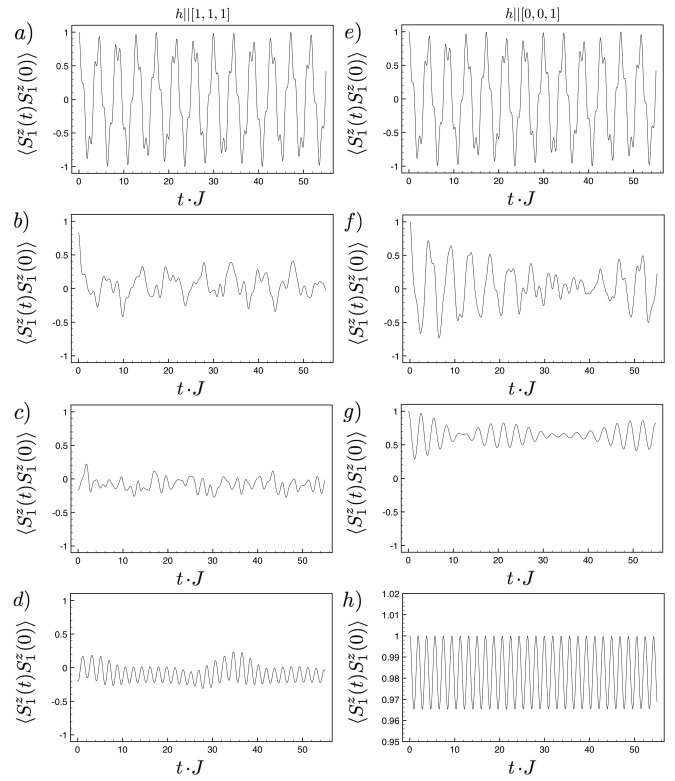


FIG. 4: A comparison of the on-site dynamical spin-spin correlations for a field pointing along  $[111]$  for AF exchange (panels a-d), with the on-site correlations for a field pointing along  $[001]$  (panels e-h). The strength of the field is:  $\theta = 0$  in panels (a,e),  $\theta \approx 0.53$  in panels (b,f),  $\theta \approx 1.07$  in panels (c,g), and  $\theta \approx 1.41$  in panels (d,h). No discernible features are evident within the intermediate range of field strengths for the  $\lambda = 1$  case (b and c), while clear nodal, beat pattern, or wave-packet features are evident and persist within a comparable range of field strength values in the  $\lambda = 0$  case (f and g). Near the highest possible field values the  $\lambda = 0$  case, (h), shows a waveform having only a single mode, consistent with the single mode seen above the zero energy mode in Fig. 3c for higher  $\theta$ . In the  $\lambda = 1$  case, (d), the waveform is a modulated sinusoid, consistent with the multiple well separated modes above the zero energy mode in Fig. 3a for higher  $\theta$ .

state along  $\hat{z}$ .

**Real time dynamics:** For  $h \parallel [001]$ , the reduction of the number of modes in the frequency response suggests that features in the dynamical spin-spin response will not be washed out by interference between multiple frequency modes. Unlike the dynamical correlations at higher  $\lambda$ , which we expect to be noisy due to the abundance of modes interfering across all  $\omega$ , we expect the waveforms at  $\lambda = 0$  to show sharp, distinct, features due to interference between a small number of modes (see Fig. 4).

We highlight this behavior in Fig. 4f, which shows a beat pattern and the formation of a node due to the destructive interference between a small number of modes of comparable energy and strength. In contrast, Fig.

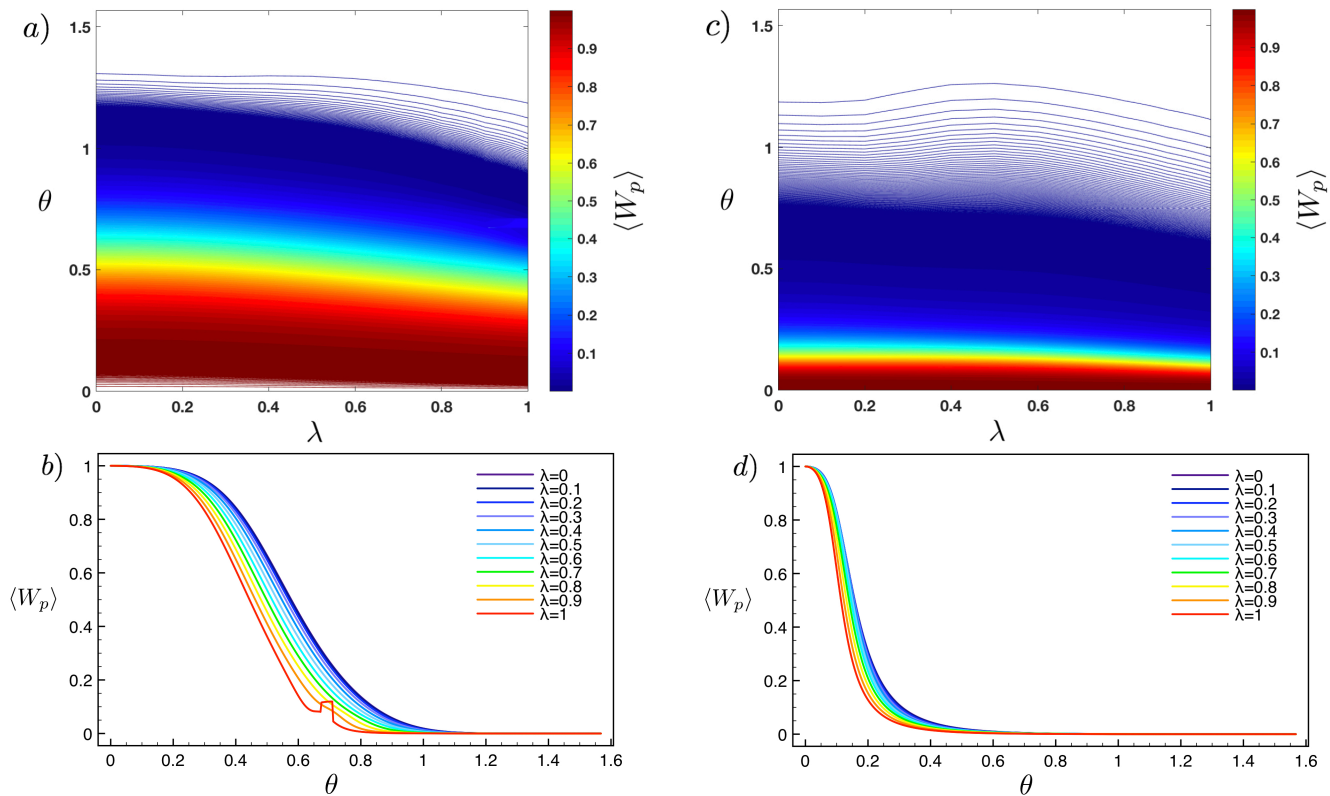


FIG. 5: Average of the plaquette operator,  $\langle W_p \rangle$ , for a finite sized cluster. Density plots for (a) AF and (c) FM exchange interactions, and corresponding line plots (b) AF and (d) FM cases, as a function of both the field strength parameter  $\theta$ , and field orientation parameter  $\lambda$ . Regions in each plot corresponding to the darkest shade of red indicate  $\langle W_p \rangle \approx 1$  as expected for the non-Abelian Kitaev spin-liquid phase. Blue and white regions correspond to  $\langle W_p \rangle \approx 0$  suggests a partially polarized phase. For AF interactions, (a), shows a clear intermediate region. For FM interactions a rather abrupt transition between the Kitaev spin liquid and the polarized phase is observed.

4b for a field along [111] does not show a similar beat pattern. At higher fields  $\theta \approx 1.07$ , the beat features, or wavepacket formation (Fig. 4g) become even more pronounced for fields along [001]. Close to the highest possible field values, near  $\theta \approx 1.41$ , the  $\lambda = 0$  waveform (Fig. 4h) is a sinusoidal pattern consistent with only a single mode of oscillation in the frequency response Fig. 3c. For the  $\lambda = 1$  case, at this same value for  $\theta$ , the waveform in Fig. 4d is a modulated sinusoidal pattern consistent with multiple, well separated modes in the frequency response in Fig. 3a.

For FM coupling,  $J < 0$ , the spectrum for all values of  $\lambda$  and  $\theta$  remains gapped (Fig.6). Similar to the AF case, we notice a reduction in the number of modes in the dynamical frequency response as the field is rotated away from [111] toward the [001] direction. This leads to a similar beat pattern appearing in the on-site, real space and time, spin-spin correlations. For more details, the FM case is presented in the appendix.

## B. Field Strength and Orientation Dependence of Plaquette Flux

To identify phase transitions, in either the AF or FM cases, we calculate the field strength and field orientation dependent average of the plaquette operator over the entire lattice,  $\langle W_p \rangle$ ,

$$\langle W_p \rangle = \frac{1}{4} \sum_{i=1}^4 \langle W_{p_i} \rangle = \frac{1}{4} \sum_{i=1}^4 \left\langle \prod_{j \in p_i} \sigma_j^{\alpha(j)} \right\rangle; \quad (7)$$

in this case over the 4 plaquettes (Fig. 5).

Because  $[W_{p_i}, H] = 0$  at  $\theta = 0$ , we see that  $\langle W_p \rangle = 1$ , exactly. Interestingly, despite  $[W_{p_i}, H] \neq 0$  for  $\theta \neq 0$ , there are finite regions as a function of  $\theta$  within which  $\langle W_p \rangle$  is very close to unity. Because  $H$  has been shown to be adiabatically connected to a Hamiltonian containing the additional three-spin exchange term  $-\kappa \sum_{ijk} \sigma_i^x \sigma_j^y \sigma_k^z$  [32], from the leading order perturbation expansion of Eq. 2, and because we can still take expectation values of the  $W_{p_i}$ 's with respect to the ground state of  $H$ , we can

reasonably interpret the range within which  $W_p \approx 1$  as corresponding to the non-Abelian Kitaev quantum spin-liquid phase. We see that, in agreement with earlier studies [29, 30], this phase appears to extend further in applied field,  $\theta$ , in the AF case than in the FM case. What is new here is the  $\lambda$ , or field orientation, dependence of this phase in each of the AF and FM cases. The Kitaev quantum spin-liquid phase across  $\theta$  increases with decreasing  $\lambda$  in both cases. In other words, changing the orientation of the field from the [111] direction to the [001] direction has the effect of expanding the region in field strength,  $\theta$ , of the Kitaev quantum spin-liquid. This effect is clearly more pronounced in the AF case than in the FM case yet, it is still non-negligible in the latter case.

In the FM case there is a sharper decrease in  $\langle W_p \rangle$ , versus  $\theta$ , than in the AF case. The partially polarized phase onsets when  $\langle W_p \rangle \approx 0$  and that happens at considerably lower values of  $\theta$  in the FM case than in the AF case. These facts, together with the observation that there is an extended region across  $\theta$  for which  $\langle W_p \rangle$  is varying continuously between unity and zero in the AF case, lends strong support for an intermediate phase between the Kitaev spin-liquid and the partially polarized phase for AF Kitaev exchange interactions.

The extent of the intermediate phase in  $\theta$  increases as the field is oriented from [111] toward [001]. Not only does the transition between the non-Abelian Kitaev spin-liquid to an intermediate phase move to a larger  $\theta$ , but the transition from the intermediate to the partially polarized phase also shifts from around  $\theta^* \approx 0.71$  at  $\lambda = 1$  to around  $\theta \approx 0.9$  at  $\lambda = 0$ .

In the FM case, Fig. 5d suggests that the transition point between the Kitaev spin-liquid and the partially polarized phase is decreases to lower  $\theta$  as a function of the field orientation parameter  $\lambda$ . We can see that in the AF case, Fig. 5c suggests that the transition between the intermediate phase and the partially polarized phase is shifted from  $\theta \approx 0.9$  at  $\lambda = 0$  to  $\theta^* \approx 0.71$  at  $\lambda = 1$ . The value of the transition at  $\lambda = 1$  is consistent with the level crossing observed in both the spectrum and the frequency response (Figs. 2a and 3a). These latter transition values are inferred by assessing the lowest bound values of  $\theta$  for which points along the  $\langle W_p \rangle$  curves are approximately zero.

#### IV. CONCLUSIONS

Recent theoretical advances concerning the nature of the ground state and excitations of the Kitaev honeycomb model have motivated experimental researchers to probe their novel properties in real materials. In particular, the temperature dependence of thermodynamic quantities and of the thermal Hall conductivity of candidate materials, as well as the dynamical response have

been suggested as a means of probing for signatures of the exotic fractionalized excitations of this particular model. In our work, we have expanded the exploration from spectroscopy to probing the nature of fractionalized excitations directly in the real-time dynamics. We propose future experiments using pump-probe THz spectroscopy on candidate materials such as  $\alpha$ -RuCl<sub>3</sub>. In these experiments, the pump excites photocarriers in the system, and the THz probe pulse measures the photoconductivity as a function of time [33]. After passing through the sample the terahertz waveform of the electric field  $E(t)$  is measured in the time domain. Based on our estimates using an exchange coupling of about 5 meV, for either the AF or FM case, we expect signatures of fractionalization to appear at time scales lying within the range  $10^{-13}$  s  $<$   $t$   $<$   $10^{-12}$  s, or for frequencies in the 1-10 THz regime.

While we bring to light new facts pertaining to the field strength and field orientation dependence of the various phases exhibited by the FM and AF Kitaev honeycomb models under an externally applied magnetic field, the nature of phase intermediate to the non-Abelian Kitaev spin-liquid phase and the partially polarized phase, in the case of AF Kitaev interactions, still requires further investigation.

#### V. ACKNOWLEDGMENTS

We would like to thank Kyusung Hwang and Kyungmin Lee for their helpful comments and discussions. We acknowledge the support of the Center for Emergent Materials, an NSF MRSEC, under Award No. DMR-1420451.

#### APPENDIX: DYNAMICAL RESPONSE FOR FERROMAGNETIC ( $J < 0$ ) COUPLINGS

We consider the effects of varying the field strength and orientation on the on-site dynamical response and real space and time spin-spin correlations of the Kitaev honeycomb model for ferromagnetic ( $J < 0$ ) interactions.

For a field along [111] a plethora of modes across all of  $\theta$  and  $\omega$ , morph into few distinct modes for a field along [001]. As in the AF case, we see two main branches onsetting at  $\omega/J \approx 1.46$  and  $\omega/J \approx 5.46$  whose average of the expectation values of the four plaquette operators is also zero, as expected. We also notice that the zero mode along  $\omega/J = 0$  becomes the dominant mode as we adjust  $\lambda$  from unity to zero. For  $\lambda = 1$ , at higher  $\theta$ , we again see a convergence of many modes into a set of well separated modes at  $\theta = \pi/2$ . For  $\lambda = 0$ , at higher  $\theta$ , we see the convergence of modes below  $\theta \approx 1.2$  into a single mode above this latter value which terminates near  $\omega/J = 4$ . Unlike the AF case, for  $\lambda = 1$ , where

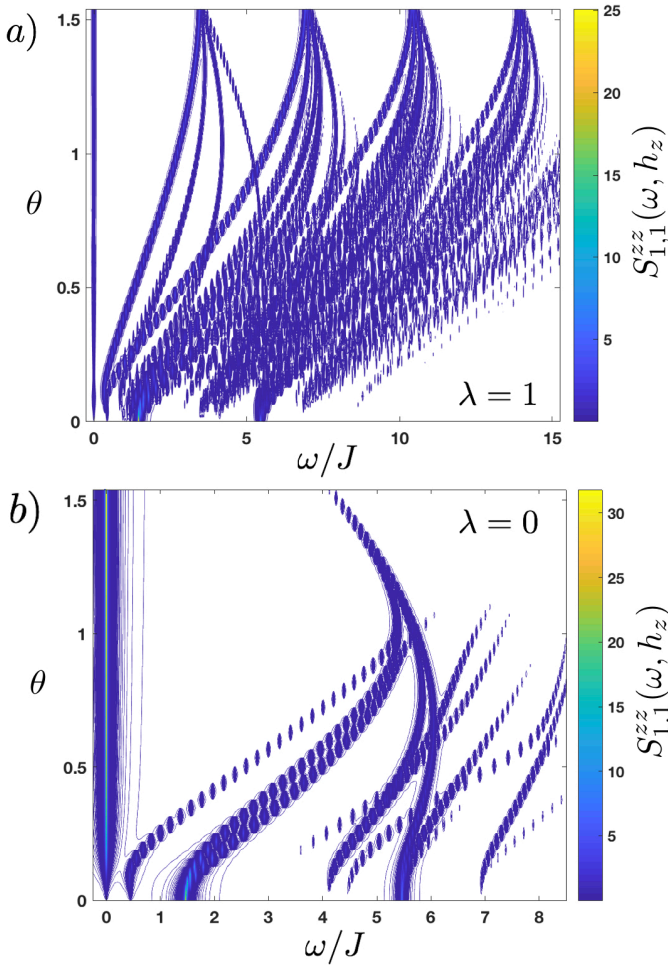


FIG. 6: The on-site dynamical response for the FM case of Eq. 2, calculated using Eq. 6, for values of the field orientation parameter a)  $\lambda = 1$  and b)  $\lambda = 0$ . Unlike the AF case, the spectrum for all values of  $\theta$  remains gapped with respect to the energy of the ground state for all values of the orientation parameter  $\lambda$ . Trajectories of the frequency modes for any orientation of the field appear streamlined such that they are seen to increase in  $\omega$  with increasing  $\theta$ . Adjusting the field orientation parameter from  $\lambda = 1$  to  $\lambda = 0$  considerably reduces the number of frequency modes detectable in the response.

we see a sharp redirection of a considerable number of modes at the transition point  $\theta \approx 0.71$ , Fig. 6a shows the general tendency of all of the modes to follow a fairly streamlined path beginning at very low  $\theta$  and extending all the way up to  $\theta = \pi/2$ .

As with the AF case, we expect the abundance of similarly weighted and energetic modes, across all  $\omega$  and  $\theta$  in Fig. 6a, to wash out any discernible features in the corresponding on-site, real space and time, spin-spin correlations. We similarly expect the fewer number of modes in Fig. 6b to yield characteristic features of interference between comparably weighted, and comparably energetic

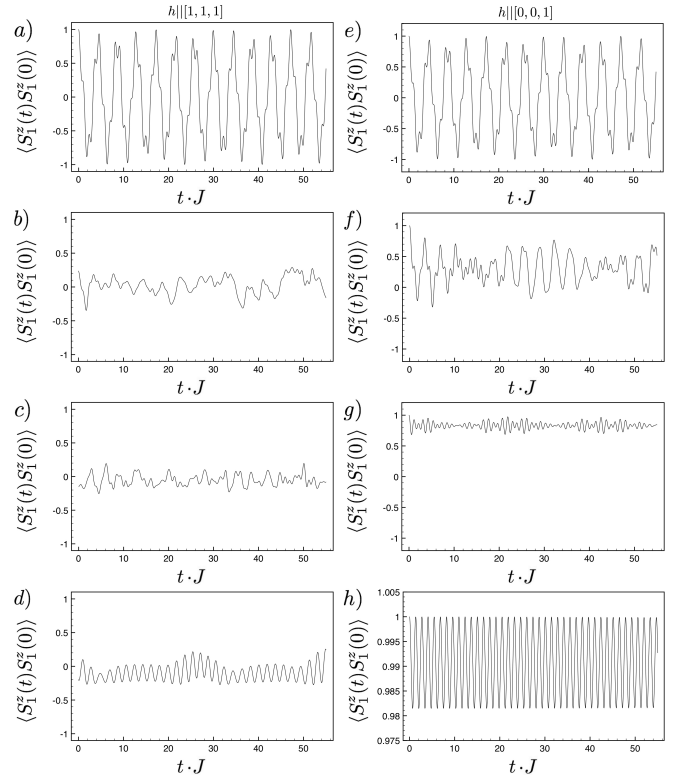


FIG. 7: A comparison of the on-site real space and time spin-spin correlations of our system under a field pointing along the [111] direction (panels a-d), with the on-site correlations corresponding to a field pointing along the [001] direction (panels e-h). The strength of the field is:  $\theta = 0$  in panels (a, e),  $\theta \approx 0.16$  in panels (b, f),  $\theta \approx 0.63$  in panels (c, g), and  $\theta \approx 1.41$  in panels (d, h). All plots correspond to the case of FM exchange interactions. The analysis provided in the caption to Fig. 4 for the case of AF interactions is analogous to our situation here, and so it is also suitable for a description of the salient features here observed.

modes.

This is reflected in Fig. 7 which compares the on-site real space and time spin-spin correlations of our system under a field pointing along the [111] direction (Fig. 7a-d), with the on-site correlations corresponding to a field pointing along the [001] direction (Fig. 7e-h). The strength of the field in these figures varies such that it is given as  $\theta = 0$  in Figs. 7a and e,  $\theta \approx 0.16$  in Figs. 7b and f,  $\theta \approx 0.63$  in Figs. 7c and g, and  $\theta \approx 1.41$  in Figs. 7d and h.

As in our prior analysis concerning the AF case, here we see no differences in signals when there is no field applied (Figs. 7a and e). There are no discernible features in the signal when a field of strength  $\theta \approx 0.16$  points along [111] (Fig. 7b), but there is a clear beat pattern forming at this same field strength for a field pointing along [001] (Fig. 7f). At the stronger field value of  $\theta \approx 0.73$ , clear wave-packets are seen to emerge in the

$\lambda = 0$  case (Fig. 7g), while the  $\lambda = 1$  orientation continues showing only a noisy signal (Fig. 7c). The waveforms observed here near the highest field values ( $\theta \approx 1.41$ ) are consistent with those observed in the AF case, where the  $\lambda = 0$  case reflects an unmodulated sinusoid consistent with having only a single mode of oscillation (Fig. 7h), and the  $\lambda = 0$  case reflects a modulated sinusoid consistent with there being multiple, well separated, competing modes.



- [1] Y. Singh and P. Gegenwart, *Phys. Rev. B* **82**, 064412 (2010), URL <https://link.aps.org/doi/10.1103/PhysRevB.82.064412>.
- [2] Y. Singh, S. Manni, J. Reuther, T. Berlijn, R. Thomale, W. Ku, S. Trebst, and P. Gegenwart, *Phys. Rev. Lett.* **108**, 127203 (2012), URL <https://link.aps.org/doi/10.1103/PhysRevLett.108.127203>.
- [3] K. W. Plumb, J. P. Clancy, L. J. Sandilands, V. V. Shankar, Y. F. Hu, K. S. Burch, H.-Y. Kee, and Y.-J. Kim, *Phys. Rev. B* **90**, 041112 (2014), URL <https://link.aps.org/doi/10.1103/PhysRevB.90.041112>.
- [4] A. Kitaev, *Annals of Physics* **321**, 2 (2006), ISSN 0003-4916, January Special Issue, URL <http://www.sciencedirect.com/science/article/pii/S0003491605002381>.
- [5] J. Knolle, D. L. Kovrizhin, J. T. Chalker, and R. Moessner, *Phys. Rev. Lett.* **112**, 207203 (2014), URL <https://link.aps.org/doi/10.1103/PhysRevLett.112.207203>.
- [6] J. Knolle, D. L. Kovrizhin, J. T. Chalker, and R. Moessner, *Phys. Rev. B* **92**, 115127 (2015), URL <https://link.aps.org/doi/10.1103/PhysRevB.92.115127>.
- [7] J. Nasu, M. Udagawa, and Y. Motome, *Phys. Rev. B* **92**, 115122 (2015), URL <https://link.aps.org/doi/10.1103/PhysRevB.92.115122>.
- [8] C. Nayak, S. H. Simon, A. Stern, M. Freedman, and S. Das Sarma, *Rev. Mod. Phys.* **80**, 1083 (2008), URL <https://link.aps.org/doi/10.1103/RevModPhys.80.1083>.
- [9] G. Jackeli and G. Khaliullin, *Phys. Rev. Lett.* **102**, 017205 (2009), URL <https://link.aps.org/doi/10.1103/PhysRevLett.102.017205>.
- [10] J. c. v. Chaloupka, G. Jackeli, and G. Khaliullin, *Phys. Rev. Lett.* **105**, 027204 (2010), URL <https://link.aps.org/doi/10.1103/PhysRevLett.105.027204>.
- [11] J. c. v. Chaloupka, G. Jackeli, and G. Khaliullin, *Phys. Rev. Lett.* **110**, 097204 (2013), URL <https://link.aps.org/doi/10.1103/PhysRevLett.110.097204>.
- [12] J. G. Rau, E. K.-H. Lee, and H.-Y. Kee, *Phys. Rev. Lett.* **112**, 077204 (2014), URL <https://link.aps.org/doi/10.1103/PhysRevLett.112.077204>.
- [13] S. M. Winter, Y. Li, H. O. Jeschke, and R. Valentí, *Phys. Rev. B* **93**, 214431 (2016), URL <https://link.aps.org/doi/10.1103/PhysRevB.93.214431>.
- [14] A. Banerjee, C. A. Bridges, J. Q. Yan, A. A. Aczel, L. Li, M. B. Stone, G. E. Granroth, M. D. Lumsden, Y. Yiu, J. Knolle, et al., *Nature Materials* **15**, 733 EP (2016), URL <http://dx.doi.org/10.1038/nmat4604>.
- [15] A. Banerjee, J. Yan, J. Knolle, C. A. Bridges, M. B. Stone, M. D. Lumsden, D. G. Mandrus, D. A. Tennant, R. Moessner, and S. E. Nagler, *Science* **356**, 1055 (2017), ISSN 0036-8075, <http://science.sciencemag.org/content/356/6342/1055.full.pdf>, URL <http://science.sciencemag.org/content/356/6342/1055>.
- [16] K. Mehlawat, A. Thamizhavel, and Y. Singh, *Phys. Rev. B* **95**, 144406 (2017), URL <https://link.aps.org/doi/10.1103/PhysRevB.95.144406>.
- [17] Y. Kasahara, K. Sugii, T. Ohnishi, M. Shimozawa, M. Yamashita, N. Kurita, H. Tanaka, J. Nasu, Y. Motome, T. Shibauchi, et al., ArXiv e-prints (2017), 1709.10286.
- [18] I. A. Leahy, C. A. Pocs, P. E. Siegfried, D. Graf, S.-H. Do, K.-Y. Choi, B. Normand, and M. Lee, *Phys. Rev. Lett.* **118**, 187203 (2017), URL <https://link.aps.org/doi/10.1103/PhysRevLett.118.187203>.
- [19] J. A. Sears, Y. Zhao, Z. Xu, J. W. Lynn, and Y.-J. Kim, *Phys. Rev. B* **95**, 180411 (2017), URL <https://link.aps.org/doi/10.1103/PhysRevB.95.180411>.
- [20] A. U. B. Wolter, L. T. Corredor, L. Janssen, K. Nenkov, S. Schönecker, S.-H. Do, K.-Y. Choi, R. Albrecht, J. Hunger, T. Doert, et al., *Phys. Rev. B* **96**, 041405 (2017), URL <https://link.aps.org/doi/10.1103/PhysRevB.96.041405>.
- [21] S.-H. Baek, S.-H. Do, K.-Y. Choi, Y. S. Kwon, A. U. B. Wolter, S. Nishimoto, J. van den Brink, and B. Büchner, *Phys. Rev. Lett.* **119**, 037201 (2017), URL <https://link.aps.org/doi/10.1103/PhysRevLett.119.037201>.
- [22] S.-H. Do, S.-Y. Park, J. Yoshitake, J. Nasu, Y. Motome, Y. S. Kwon, D. T. Adroja, D. J. Voneshen, K. Kim, T. H. Jang, et al., *Nature Physics* **13**, 1079 EP (2017), URL <http://dx.doi.org/10.1038/nphys4264>.
- [23] J. Zheng, K. Ran, T. Li, J. Wang, P. Wang, B. Liu, Z.-X. Liu, B. Normand, J. Wen, and W. Yu, *Phys. Rev. Lett.* **119**, 227208 (2017), URL <https://link.aps.org/doi/10.1103/PhysRevLett.119.227208>.
- [24] A. Banerjee, P. Lampen-Kelley, J. Knolle, C. Balz, A. A. Aczel, B. Winn, Y. Liu, D. Pajerowski, J. Yan, C. A. Bridges, et al., *npj Quantum Materials* **3**, 8 (2018), URL <https://doi.org/10.1038/s41535-018-0079-2>.
- [25] R. Hentrich, A. U. B. Wolter, X. Zotos, W. Brenig, D. Nowak, A. Isaeva, T. Doert, A. Banerjee, P. Lampen-Kelley, D. G. Mandrus, et al., *Phys. Rev. Lett.* **120**, 117204 (2018), URL <https://link.aps.org/doi/10.1103/PhysRevLett.120.117204>.
- [26] R. Yadav, N. A. Bogdanov, V. M. Katukuri, S. Nishimoto, J. van den Brink, and L. Hozoi, *Scientific Reports* **6**, 37925 EP (2016), URL <http://dx.doi.org/10.1038/srep37925>.
- [27] G.-W. Chern, Y. Sizyuk, C. Price, and N. B. Perkins, *Phys. Rev. B* **95**, 144427 (2017), URL <https://link.aps.org/doi/10.1103/PhysRevB.95.144427>.
- [28] S. M. Winter, K. Riedl, D. Kaib, R. Coldea, and R. Valentí, *Phys. Rev. Lett.* **120**, 077203 (2018), URL <https://link.aps.org/doi/10.1103/PhysRevLett.120.077203>.
- [29] Z. Zhu, I. Kimchi, D. N. Sheng, and L. Fu, ArXiv e-prints (2017), 1710.07595.
- [30] M. Gohlke, G. Wachtel, Y. Yamaji, F. Pollmann, and Y. B. Kim, *Phys. Rev. B* **97**, 075126 (2018), URL <https://link.aps.org/doi/10.1103/PhysRevB.97.075126>.
- [31] E. H. Lieb, *Phys. Rev. Lett.* **73**, 2158 (1994), URL <https://link.aps.org/doi/10.1103/PhysRevLett.73.2158>.
- [32] H.-C. Jiang, Z.-C. Gu, X.-L. Qi, and S. Trebst, *Phys. Rev. B* **83**, 245104 (2011), URL <https://link.aps.org/doi/10.1103/PhysRevB.83.245104>.
- [33] J. Zhang and R. Averitt, *Annual Review of Materials Research* **44**, 19 (2014), <https://doi.org/10.1146/annurev-matsci-070813-113258>, URL <https://doi.org/10.1146/annurev-matsci-070813-113258>.